

# Density functional study of Ni bulk, surfaces and the adsorbate systems Ni(111) $(\sqrt{3} \times \sqrt{3})R30^\circ\text{-Cl}$ , and Ni(111) $(2 \times 2)\text{-K}$

K. Doll

*Institut für Mathematische Physik, TU Braunschweig, Mendelssohnstraße 3, D-38106 Braunschweig*

Nickel bulk, the low index surfaces and the adsorbate systems Ni(111)  $(\sqrt{3} \times \sqrt{3})R30^\circ\text{-Cl}$ , and Ni(111) $(2 \times 2)\text{-K}$  are studied with gradient corrected density functional calculations. It is demonstrated that an approach based on Gaussian type orbitals is capable of describing these systems. The preferred adsorption sites and geometries are in good agreement with the experiments. Compared to non-magnetic substrates, there does not appear to be a huge difference concerning the structural data and charge distribution. The magnetic moment of the nickel atoms closest to the adsorbate is reduced, and oscillations of the magnetic moments within the first few layers are observed in the case of chlorine as an adsorbate. The trends observed for the Mulliken populations of the adsorbates are consistent with changes in the core levels.

## I. INTRODUCTION

Adsorption on surfaces is one of the main focuses in surface science due to the enormous importance of topics such as corrosion or catalysis. A huge number of experiments has been performed to understand these processes. In addition, theoretical studies have become capable of modelling the adsorption process.

The adsorption of alkali metals or halogenes on metallic surfaces may be considered as two prototypes of adsorption processes. They are fairly simple and experimentally well studied. However, there have been quite a few surprises. For example, the occupancy of top sites by alkali metals as adsorbates was unexpected (for reviews, see references 1–3 and more general, reference 4). Halogens are another type of adsorbate which is experimentally well studied. On close-packed (111) surfaces, they usually occupy the face centered cubic (fcc) hollow site, and in a few systems a partial occupancy (around 15-25%) of hcp (hexagonal close-packed) sites has also been observed<sup>5,6</sup>. In addition, there is now a growing set of simulations for halogens on metallic surfaces (e.g. chlorine<sup>7–9</sup>, bromine<sup>10,11</sup> or iodine<sup>12</sup>). Both for alkali metals and for halogens as adsorbates, there are general questions such as the geometry, binding energies, diffusion barriers, charge transfer and the binding mechanism.

Magnetic surfaces pose additional difficulties and questions such as how the magnetic moment changes after adsorption. It is thus an interesting question which insights simulation can give for these systems. Nickel surfaces and adsorption thereon have been well studied by experimental groups and thus are a prototype system for a computer simulation. For example, hydrogen on Ni(111)<sup>13</sup>, benzene on Ni(111)<sup>14</sup>, CH<sub>3</sub> dehydrogenation on Ni(111)<sup>15</sup> or CO on Ni(110)<sup>16</sup> adsorption have been simulated recently. The present article will deal with the simulation of alkali and halogen adsorption, with Cl and K as examples.

The intention of this article is to give a broad overview over nickel and the adsorbate systems. The computational technique is based on a local basis set of Gaussian type functions. As nowadays most calculations, especially for metals, rely on plane-waves, the following section II was devoted to the fairly simple systems of Ni bulk and the low index surfaces. This way, it will be demonstrated that results from a code based on Gaussian type orbitals reproduce the ones from plane-wave codes. In sections III and IV, the results for chlorine and potassium adsorption are presented, respectively. Finally, the results are summarized and discussed. Additional details on the calculations are given in the appendix.

## II. NI BULK AND LOW INDEX SURFACES

### A. Computational Parameters

A local basis set formalism was employed where the basis functions are Gaussian type orbitals centered at the atoms as implemented in the code CRYSTAL<sup>17</sup>. The calculations were done with spin-polarization, using the gradient corrected functional of Perdew, Burke and Ernzerhof (PBE)<sup>18</sup>, and in some additional calculations the gradient corrected functional by Perdew and Wang (PW)<sup>19</sup>. These functionals perform actually nearly identical (see, e.g. references 18, 20, or with the CRYSTAL code for Ag<sup>8</sup>), and also in the present article the results with both functionals are very similar. The PBE functional may be viewed as slightly favorable because it was designed to have a simpler form and derivation, and already revised versions exist (see, e.g., reference 20).

The nickel basis set from reference 21 was employed, with the innermost  $[4s3p1d]$  exponents being unchanged. In addition, 2  $sp$  functions with exponent 0.63 and 0.13 and a  $d$ -function with exponent 0.38 as optimized in calculations for the bulk were used, so that the basis set as a whole was of the size  $[6s5p2d]$ . The chlorine and potassium basis sets were the ones used in previous studies on Cl/Cu(111) and K/Cu(111), respectively<sup>7,22</sup>. For the calculations on the free atoms, enhanced basis sets with additional diffuse functions were used<sup>23</sup>. For the numerical integration, the potential was fitted with auxiliary basis sets (for Cl the same as in reference 7, for K as in reference 22, and for Ni the same as for Cu in reference 22). A  $\vec{k}$ -point net with  $16 \times 16$  points in the surface Brillouin zone and  $16 \times 16 \times 16$  points for the bulk was used. A smearing temperature of  $0.001 E_h$  was applied to the Fermi function ( $1E_h=27.2114 \text{ eV}=315773 \text{ K}$ ). This value for the temperature was chosen relatively low to ensure that the magnetic moment is not artificially modified by a too high value. For more details and tests on the computational parameters and basis sets, see also the appendix.

The calculation of the charge and spin population is based on the Mulliken population, which is actually due

to McWeeny<sup>24,25</sup> (see also reference 26). The Mulliken charge is defined as  $\sum_{\mu \in A} \sum_{\nu} P_{\mu\nu} S_{\nu\mu}$  (with density matrix  $P$ , overlap matrix  $S$  and  $A$  the set of basis functions for which the population is computed). In the case of the spin population the density matrix for the corresponding spin polarization has to be used. This type of population analysis thus depends on the basis sets. It will be questionable if basis sets of different quality are used for various atoms: if one basis set is very small and the other very large, and especially if the larger basis set also has more diffuse exponents (i.e. smaller exponents, which results in a Gaussian with a relatively large spatial extension), the larger basis set may describe a part of the charge of the atom with the smaller basis set as well, and thus the Mulliken charge will be artificially large for the atom with the larger basis set. It is thus important that balanced basis sets are used. Concerning the Mulliken populations computed in this article, the population can be expected to be fairly reliable in the case when identical basis sets are used for the various atoms in a slab, so that the magnetic moments computed for the various layers of a nickel slab should not have a too large error due to the choice of the basis set. Also, comparing results for various adsorption sites should not be too unreasonable, because the basis sets for the systems are identical. This means, that, for example, a relative comparison of the Mulliken charge for chlorine on the fcc site with the charge on the top site should not be too unrealistic, although the absolute value of the Mulliken charge may have a larger error. A more difficult issue is however, to compare the chlorine charge for Cl/Ni(111) with the one for Cl/Ag(111) or Cl/Cu(111) because different basis sets for the metals are used and because of the different geometries.

The adsorbate systems Ni(111) ( $\sqrt{3} \times \sqrt{3}$ )R30°-Cl and Ni(111)(2 × 2)-K were modeled with a slab consisting of 3 nickel layers and the adsorbate layer, with the adsorbate layer on one side of the slab. The model is truly two-dimensional and not periodically repeated in the third dimension. This is different from the more common approach where periodicity in three dimensions is used, and a number of vacuum layers is required to separate the periodically repeated slabs. In the latter case, this also introduces an artificial electrical field due to the periodic boundary conditions in the third dimension, which is usually compensated for by an additional dipole field<sup>27</sup>. The approach used by the CRYSTAL code for slabs avoids this artificial field as there are no periodic boundary conditions in the third dimension, and thus there is no correction required, and there is no parameter for the number of vacuum layers either. The simulation was performed for the fcc, hcp, bridge and top site (see figures 1 and 2). To ensure the stability of the results with respect to the number of layers, additional calculations with thicker slabs were performed for the systems Cl/Ni(111) (which is easier to converge than K/Ni(111)).

## B. Properties of bulk Ni and clean Ni surfaces

Results for cohesive properties of bulk Ni are displayed in Table I. The computed values in this work reproduce essentially the ones obtained with the gradient corrected functional of Perdew and Wang, with the plane-wave pseudopotential method<sup>28</sup>. The binding energy is overestimated, compared to the experiment. Also, the energy splitting between  $d^8s^2$  and  $d^9s^1$  is not well reproduced (the  $d^9s^1$  state should be lower by -0.03 eV, after averaging the experimental energies over spin-orbit components<sup>29,30</sup>). This is however, not a serious problem, as the orbital occupancy in the solid is different from the atom and thus the error cancellation does not work too well, and a density functional description may be too crude to describe these effects. The splitting between  $d^8s^2$  and  $d^9s^1$  state is a problem well known in quantum chemistry. The relativistic effect to the energy splitting between these states was computed to be of the order of 0.3 eV<sup>30,31</sup> (i.e. in a non-relativistic calculation as the present one, the splitting should be -0.33 eV instead of -0.03 eV) and thus is not negligible. With highly accurate configuration interaction schemes<sup>31</sup>, the calculated splitting is -0.18 eV; i.e. there is still an error of 0.15 eV, compared to the experimental splitting, after relativistic effects were subtracted from the experimental value. The value computed here ( $-0.035 E_h \hat{=} -0.95$  eV); is in reasonable agreement with other results from literature, e.g. in the range of -1.1 to -1.2 eV, both at the level of the local density approximation (LDA) and the level of the generalized gradient approximation (GGA), with the PW functional<sup>28</sup>. This difficulty in obtaining the correct energy splitting between  $d^{n-1}s^1$  and  $d^{n-2}s^2$  was also identified as a general problem for the transition metals<sup>32</sup>, with the LDA, where a bias towards  $d^{n-1}s^1$  of  $\sim 1$  eV was found. With a different gradient corrected functional (B-LYP), an energy splitting of -0.82 eV was computed<sup>33</sup>. There is, however, no reason why other properties should be affected by this problem.

The band structure is displayed in figure 3. It agrees well with the early tight binding<sup>34,35</sup> or augmented plane wave<sup>36</sup> results, and thus supports the validity of the applied approach, relying on Gaussian type orbitals.

Surface formation energies (in  $E_h$  per surface atom) of the clean, unrelaxed surfaces are displayed in Table II. The surfaces were modeled with a finite number of Ni layers (typically from 1 to 9). The PBE energies obtained here are within literature values. For the (111) surface, the surface energy was additionally computed with the Perdew-Wang functional, and is identical to the one with the PBE functional.

Finally, in Table III, the magnetic moments of the layers of the unrelaxed slabs are given. In all cases, they were computed using a 9 layer slab. They are in good agreement with literature values. For the (111) surface it is found that the second layer in the slab has the highest magnetic moment and not the top layer, in agree-

ment with two of the published articles. For comparison, for the (111) surface, relaxation of the top layer was additionally taken into account. This resulted in a small inwards contraction by  $0.03 \text{ \AA}$ , which is consistent with experimental<sup>37</sup> and theoretical<sup>38</sup> findings. The magnetic moments were virtually unchanged, and thus relaxation does not seem to explain why in one publication it was observed that the outermost layer should have the highest moment<sup>38</sup>. For comparison, also the Perdew-Wang functional was used to compute the moments of the unrelaxed (111) surface, and the results of the PBE functional were essentially reproduced. As explained earlier, the calculation of the magnetic moments is based on the Mulliken population analysis. The error should, however, not be too large as identical basis sets are used for all the nickel atoms of the slabs.

### III. CL ON THE NI(111) SURFACE

As a first adsorbate system, the adsorption of Cl on the Ni(111) surface was investigated. This system was studied experimentally with LEED (low energy electron diffraction), Auger electron spectroscopy, work function measurements and flash desorption<sup>39</sup>, surface extended X-ray absorption fine structure (SEXAFS) and soft X-ray standing wave (XSW)<sup>40,41,5</sup>, and angle-resolved photoemission fine-structure measurements (ARPEFS)<sup>42</sup>. At low coverages there were indications of a  $(2 \times 2)$  pattern, followed by a  $(\sqrt{3} \times \sqrt{3})R30^\circ$  structure, and a complex  $\begin{pmatrix} 2 & 1 \\ 4 & 7 \end{pmatrix}$  pattern. The  $(\sqrt{3} \times \sqrt{3})R30^\circ$  structure is the one which has been extensively studied experimentally and thus also the calculations will focus on this pattern. There was agreement that the fcc hollow was the preferred site (with an fcc:hcp population ratio of around 85:15<sup>5</sup>, and the Cl-Ni bond length was measured to be  $2.40 \pm 0.04 \text{ \AA}$ <sup>40</sup>,  $2.33 \pm 0.02 \text{ \AA}$ <sup>41</sup> or  $2.332 \pm 0.006 \text{ \AA}$ <sup>42</sup>. This corresponds to an interlayer distance of  $1.92 \text{ \AA}$ <sup>40</sup>,  $1.83 \text{ \AA}$ <sup>41</sup> or  $1.837$ <sup>42</sup>. The first nickel layer was found to be practically unrelaxed in two experiments<sup>40,41</sup>, whereas in the other article, a 5% contraction with respect to the bulk value was deduced<sup>42</sup>.

It is thus an interesting issue to compare with results from the simulations. These results are presented in Table IV. A structural optimization was performed with 3 and 4 nickel layers. An additional single point calculation with 5 nickel layers was performed for fcc and hcp site, where the geometry from the thinner slabs was used, with one additional nickel layer at the distance corresponding to the bulk. The vertical positions of the chlorine adatoms and of the first nickel layer were optimized. Lateral relaxations are not possible for fcc and hcp site. As bridge and top site are much higher in energy, lateral relaxations were not taken into account for these sites either. Comparing the data for three and four layers, we see that the geometry is well converged, and the difference in the energy splitting between the sites

is within what is expected as the numerical noise (e.g. fcc vs. hcp site, the energy splitting is  $0.7 mE_h$  with three nickel layers,  $0.2 mE_h$  with four layers, and  $0.6 mE_h$  with five layers). Firstly, we note that the fcc hollow is indeed found to be lowest in energy, with the hcp hollow being nearly degenerate at an energy difference of only  $0.2-0.7 mE_h$  ( $\sim 60-220$  K). Although the numerical noise is not negligible when energy differences on this small scale are computed (see appendix), this energy difference would be compatible with the simple thermodynamic estimate given in reference 6, with copper as substrate. The bridge site is higher in energy by  $\sim 3 mE_h$  (or more than 900 K), the top site by  $18 mE_h$ , and thus thermodynamically fcc and hcp sites are clearly favored. The energy splitting between fcc (or hcp site), and the bridge site, may also be a crude estimate for the diffusion barrier from one threefold-hollow site to another one. These findings are actually very similar to those<sup>7-9</sup> for  $\text{Cu}(111)(\sqrt{3} \times \sqrt{3})\text{R}30^\circ\text{-Cl}$  and  $\text{Ag}(111)(\sqrt{3} \times \sqrt{3})\text{R}30^\circ\text{-Cl}$ , and also for the system  $\text{Ag}(111)(1 \times 1)\text{-O}$ <sup>43</sup>: on the (111) surface, the highly coordinated sites are clearly lowest in energy for adsorbates with a small radius. The bond lengths from chlorine to the nearest nickel  $d_{\text{Cl-Ni nn}}$  also increase with increasing coordination number and the binding energy increases with increasing coordination number, as is to be expected from Pauling's argument<sup>44</sup>: one strong Cl-Ni bond in the case of the top site will be shorter than the three weaker bonds in the case of fcc and hcp, but the three bonds as a whole are energetically more favorable. The computed bond length agrees well with the values from the literature<sup>40-42</sup>.

There are two different experimental results for the interlayer distance between first and second nickel layer. The computed value from this article agrees very well with the experimental from references 40, 41, whereas the large contraction of  $0.10 \text{ \AA}$ <sup>42</sup> with respect to the bulk appears to be unlikely. A smaller contraction would also be in line with simulations with Cu or Ag as substrate<sup>7-9</sup>.

An effective radius for Cl on Ni(111) could be computed by subtracting an effective nickel radius of  $\frac{3.53}{2\sqrt{2}} \text{ \AA}$  from the bond length  $d_{\text{Cl-Ni nn}}$  of  $2.34 \text{ \AA}$ . This would result in a radius of  $1.09 \text{ \AA}$ , in agreement with the computed values<sup>7,8</sup> for Cl on Cu(111) ( $1.12 \text{ \AA}$ ) or Cl on Ag(111) ( $1.17 \text{ \AA}$ ). Thus the radius for Cl is intermediate between the atomic ( $0.99 \text{ \AA}$ ) and ionic ( $\text{Cl}^-$ ;  $1.81 \text{ \AA}$ )<sup>45</sup>. The bond length  $d_{\text{Cl-Ni nn}}$  is also in agreement with experimental values for systems with similar atomic radii for the substrate (e.g., bond lengths of  $2.39 \text{ \AA}$  for the substrate Cu(111)<sup>46</sup>,  $2.38 \text{ \AA}$  for Rh(111)<sup>47</sup>,  $2.39 \text{ \AA}$  for Pd(111)<sup>48</sup>).

In Table V, the Cl population is displayed. The data is extracted from the calculations where three nickel layers were used to model the substrate, but it is virtually identical to the data obtained with four nickel layers. The negative charge is largest for the top site, smaller for the bridge site and smallest for hcp and fcc site. This is consistent with the position of the  $3s$  core eigenvalue

relative to the Fermi level, which is lowest for hcp and fcc, increasing for bridge and largest for the top site (because the negative charge of the chlorine adsorbate is increasing and thus the core levels are destabilized). Note that the core level for majority spin is also slightly lower (by  $\sim 0.002 E_h$ ) than for minority spin. The density of states is visualized in figure 4, projected on the chlorine basis functions, and projected on all basis functions (i.e. the total density of states). The different occupancy of the two spin states becomes visible. Note that the chlorine spin is mainly due to the different population of the second and third  $p$ -shell, and not of the fourth (if we order the shells according to the size of the exponents, starting with the highest). This means that the outermost and thus most diffuse exponent does not carry a huge spin and thus the chlorine spin is not an artifact of the Mulliken population (if the spin was on the most diffuse function only, one might argue that this basis function also describes the spin on the nickel atoms and thus the Mulliken population analysis would be questionable).

The computed Mulliken charge is also in agreement with the experimental estimates of 0.1 to 0.2  $|e|$  derived from work function measurements<sup>39</sup>. The overlap population  $\sum_{\mu \in A} \sum_{\nu \in B} P_{\mu\nu} S_{\nu\mu}$  (with density matrix  $P$ , overlap matrix  $S$  and  $A$ ,  $B$  the set of basis functions of atoms  $A$  and  $B$  for which the overlap population is computed) is 0.09 for Cl and the nearest nickel atoms. This may indicate that there is no evidence for a strong covalent contribution to the binding mechanism, similar to non-magnetic substrates<sup>7,8,22,49</sup>, and now also in the case of a magnetic substrate. For comparison, the overlap population between two nearest nickel atoms in the top nickel layer is 0.10. However, this data should not be over-interpreted, and the overlap population should rather be viewed as a rough qualitative measure and not a quantitative measure for covalency. Another indication that the covalency is not strong might be that in the case of the bridge site, where  $p_x$  and  $p_y$  orbitals do not have the same occupancy, the orbital with the larger overlap with the neighboring nickel atoms ( $p_x$  in our choice of geometry) has a slightly smaller population than  $p_y$  (the total Cl  $p$  population is 3.73 for  $p_x$ , versus 3.82 for  $p_y$ ).

Charge density, charge density difference and spin density are visualized in figure 5. As usual, the charge density difference is more informative as the charge density. The transfer from the top nickel layer to the chlorine atom becomes obvious. In contrast to the charge density, the spin density also offers more information: it is very interesting that the spin density varies relatively strong still for the atoms in the third layer. This is confirmed by the data from Mulliken population analysis for the spin (table VI). The magnetic moments depend relatively strong on the number of layers, and the analysis has been performed by extracting the data from a single-point calculation for a slab with 5 nickel layers, with an identical geometry as for the 3-layer slab, i.e. the additional layers were added at a distance as in the bulk.

The data is presented in such a way that one number

is given, if all the atoms in a layer have the same distance to the chlorine atom, and two numbers, if there are two different distances for the atoms in one layer possible. For example, in the case of the fcc site, looking at the atoms in the first or second layer, all three nickel atoms within a supercell have the same distance to the adsorbed chlorine. However, in the third layer there will be one atom which is closer than the other two. The population of this closer atom (0.59) is displayed in the left column of the results for the 3<sup>rd</sup> layer, the data for the other two atoms (0.64) in the right column.

It is interesting to note that those nickel atoms in the first layer which are closer to the chlorine atom have a reduced magnetic moment. This is strongest in the case of the top site where the atom vertically under the chlorine has its population reduced to 0.55, versus a moment of 0.76 for the other two atoms. It is also apparent for the bridge site (0.66 vs 0.73), and in the case of fcc and hcp site the data is identical because the nickel atoms in the first layer are identical by symmetry.

In the second layer, the spin population is higher for those atoms which are closer to the adsorbate (this is possible for the hcp and bridge structure). In the third layer, again those atoms which have a shorter distance to the adsorbate, have their moment reduced. These oscillations are still visible in the fourth and fifth layer.

Although this data depends relatively strongly on the number of layers, it becomes apparent that there are oscillations in the spin density. It is also interesting to compare with the total charge: the latter quantity is virtually constant within the layers, from the second layer on, and has a value identical to that of a clean slab from the third layer on (also table VI). Only in the first layer, the atom(s) closer to the chlorine adsorbate have a slightly higher charge (i.e. more electronic charge) than the atom(s) which are further apart (visible for bridge and top site).

Finally, the chlorine adsorbate has a magnetic moment of  $\leq 0.1$  for all sites (the smallest value for the top site). The moment is always parallel to the nickel spin.

It is interesting to note that in the simulations for CO on Ni(110)<sup>16</sup>, it was also found that the moment of the atom(s) closest to the CO was reduced.

#### IV. K ON THE NI(111) SURFACE

In addition, the system Ni(111)(2 × 2)-K was studied with this approach. Experimentally, in a LEED study at various coverages, this was found to be the only commensurate structure<sup>50</sup>. In a further LEED study<sup>51,52</sup>, the top site was found to be occupied, with a K-Ni distance of  $2.82 \pm 0.04$  Å, a vertical rumpling of the first Ni layer of 0.12 Å, and a lateral displacement of 0.06 Å of the three nickel atoms in the top layer which are not vertically under the K adsorbate. The adsorption site was later confirmed in SEXAFS measurements<sup>53</sup>, and a



larger bond length of  $2.92 \pm 0.02$  Å was obtained. With the same technique, also the bond length for the system K/Cu(111) was computed and deduced to be by  $0.06 \pm 0.04$  Å larger. From ARPEFS<sup>54</sup>, a top site adsorption with K-Ni bond-length of  $3.02 \pm 0.01$  Å was obtained. In addition, the first to second layer spacing was reduced by  $0.13$  Å to  $1.90 \pm 0.04$  Å, but no substrate rumpling in the top layer was observed. Lateral displacements were not found either ( $0.00 \pm 0.09$  Å) in this experiment. Finally, photoelectron diffraction (PhD)<sup>55</sup> resulted in a bond length of  $2.87 \pm 0.06$  Å, and a reduced first to second layer distance of  $1.86 \pm 0.06$  Å was observed, with virtually no rumpling in the first layer ( $0.01 \pm 0.09$  Å).

The experiments thus consistently support the top site as the adsorption site, but the geometrical parameters are not identical. Moreover, a comparison with the system K/Cu(111) is very interesting, so that the influence of the partially occupied *d*-bands can be investigated.

The results of the simulations are summarized in Table VII, with geometrical parameters as defined in figure 6. Initially, the potassium position and the position of the top nickel layer was optimized (i.e. the uniform relaxation of the top nickel layer). In a second step, a vertical rumpling of the nickel atoms in the top layer was allowed, as this is expected to be important for the top site occupancy. A further refinement would have been the additional possibility of lateral relaxations. These lateral relaxations were, however, found to be of minor importance for the related system K/Ag(111), where the energy was lowered by the order of typically  $0.1 - 0.2$   $mE_h$ , when these relaxations were allowed<sup>49</sup>. Thus, lateral relaxations were taken into account additionally only for the top site, which was found to be lowest in energy, and in order to compare with the experimental data for the lateral displacement.

Firstly, the top site is found to be the most favorable site. This is in agreement with the experimental findings<sup>51–53</sup>. By disabling the possibility of substrate rumpling, it is also demonstrated that substrate rumpling is crucial for top site occupancy, as it lowers the energy by  $1.6$   $mE_h$ , but only  $0.4$   $mE_h$  for the other sites. These findings are actually similar to the system K/Cu(111)<sup>22</sup>. The top site thus becomes the most stable site because the nickel atom underneath is pushed into the substrate relative to its neighbors and the potassium with its relatively large radius thus also overlaps more with the second nearest nickel neighbors.

The computed bond length ( $2.79$  Å) is also very similar to K/Cu(111) ( $2.83$  Å)<sup>22</sup> so that these calculations do not indicate a major difference compared to Cu. Experimentally, using the same technique for both adsorbate systems, it was measured to be slightly shorter and it was speculated that this was due to greater adatom-substrate interactions involving the partially filled Ni *d* bands<sup>53</sup>. The possibility of a lateral displacement of the nickel atoms as observed experimentally ( $0.06$  Å)<sup>51</sup> was investigated. However, this could not be confirmed and the energy was found to be lowest for the case where this

lateral displacement is exactly zero.

Bridge, fcc and hcp site are found to be energetically degenerate. The fact that all the sites are energetically very close (e.g. much closer than in the case of chlorine) is consistent with earlier findings<sup>27,22,49</sup> and was explained due to the large radius of the adsorbate which makes it experience only a small substrate electron density corrugation<sup>27</sup>. This small energy splitting between the various sites is also consistent with the experiment because of various observations<sup>53</sup>: firstly, the SEXAFS data indicated enhanced in-plane motion resulting from a wide and shallow potential well. Secondly, no SEXAFS signal was observed for low coverages below 0.13 monolayers. It was thus argued that lateral motion was essentially hindered by the presence of other adatoms. Finally, with increasing temperature (already in the range of 120-145 K) the SEXAFS amplitude was found to decrease. This was explained due to the occupancy of other sites, which leads to a destructive interference.

The bond length  $d_{\text{K-Ni nn}}$  increases with the number of nearest nickel neighbors in the order top, bridge, fcc and hcp. The effective radius of the potassium adsorbate is  $2.79 - \frac{3.53}{2\sqrt{2}} \text{ \AA} = 1.54 \text{ \AA}$  for the top site. This number is in good agreement with experimental values for potassium when occupying the top site<sup>1</sup>, or the computed value for K/Cu(111) (1.55 Å<sup>22</sup>).

Looking at the populations in Table V, we see that they ( $\sim 0.3 |e|$ ) are very similar for all considered sites, only for the top site the charge is slightly less positive. In agreement with this, the core eigenvalues of the 3s and 3p orbital are virtually independent of the site. The core levels are identical for both spin polarizations which agrees with the finding that the magnetic moment of the potassium adatoms is negligible (see below). In the calculations for K/Ag(111)<sup>49</sup>, it was recently shown that the adsorbate charge and thus also the core eigenvalue (and other properties such as the bond length) change with the coverage. Such a change in the core eigenvalues was observed experimentally for alkali metals on metallic surfaces, e.g. for the systems Na/Cu(111) and Na/Ni(111)<sup>56</sup>, or for alkali metals on Ru(100)<sup>57</sup> or W(110)<sup>58</sup>.

The overlap population is  $\sim 0.03$  for K and the nearest nickel atom, so that there is also in this case no evidence for a strong covalent contribution to the binding mechanism.

The density of states is displayed in figure 7. The integrated density of states, when projected on the potassium basis functions, differs so little for majority and minority spin that there is nearly no magnetic moment. For the top site, the spin is even antiparallel to the nickel sites, in contrast to the other sites (and in contrast to chlorine).

Again, the charge density is not very informative, and it is more interesting to look at the charge density difference (figure 8). Electrons have flown from the adsorbate mainly to the top nickel layer (and a relatively large part to the atom vertically under the potassium adatom). Thus, the charge of the potassium overlayer

has decreased. It is apparent that the spin density of the nickel atom vertically under the top atom is slightly lower than the spin density of its neighbors in the same layer, as the contours are closer to the nucleus. This is confirmed in the Mulliken spin population (table VIII). Again, those atoms in the top layer which are closest to the potassium adsorbate, have their moment reduced. No noteworthy variation is found in the second and third nickel layer, and the values for the spin population are very close to the ones for the clean Ni slab. The moment of the potassium adsorbate is negligible, as its magnitude is  $\leq 0.003$ . Also, the charge only varies in the first layer, and already the second and third layer have charges which are identical to that of a clean slab.

There are thus no oscillations of the spin population beyond the first nickel layer, probably because the potassium magnetic moment is much smaller than that of chlorine.

## V. SUMMARY

We have studied Ni bulk, the clean low index surfaces and the adsorption of chlorine and potassium on the Ni(111) surface.

The results for the adsorption geometry confirm the experimental findings. It turns out that there is no huge difference to copper as substrate; the preferred adsorption site and energies are very similar.

The reason for the preference of the top site for K is substrate rumpling which helps to increase the overlap of the K adsorbate with the second nearest nickel neighbors. This rumpling is thus crucial for the site preference. In the case of chlorine, the threefold hollow sites are very close in energy. In general, the adsorbate atoms prefer sites with the highest possible coordination number, or they try to increase the overlap to neighboring atoms by substrate rumpling.

There appear to be no strong covalent contributions to the binding so that the mechanism appears to be mainly an ionic bond (although the charge transfer is rather small), and in the case of potassium, additionally a metallic binding mechanism. However, the quantitative analysis of the binding mechanism is certainly difficult. The computed charges seem to be fairly reliable, but the overlap population is probably only a qualitative tool to estimate the degree of covalency.

Charges and core levels were found to be consistent, i.e. with increasing negative charge of the adsorbate, the core levels of the adsorbate are slightly destabilized. It is also demonstrated that the magnetic moments computed with the help of the Mulliken population analysis agree well with data from other schemes, e.g. pseudopotential plane wave. The calculation of work functions, however, seems to be difficult with a local basis set and the results are strongly basis-set dependent.

Finally, the magnetic moment of those nickel atoms

closest to the adsorbate are always reduced. Oscillations of the spin population within one nickel layer are notable for the first three layers for Cl/Ni(111), but only for the first nickel layer for K/Ni(111), probably because of the very small magnetic moment of the potassium adsorbate, compared to chlorine.

## VI. ACKNOWLEDGMENTS

All the calculations were performed at the computer centre of the TU Braunschweig (Compaq ES 45).

## APPENDIX A: TEST OF COMPUTATIONAL PARAMETERS

The calculations require various sets of parameters, with the most important being: a finite number of  $\vec{k}$ -points, a finite temperature to smoothen the integrand and thus to facilitate the numerical integration of the exchange-correlation functional, basis set parameters, and truncation schemes to reduce the number of matrix elements (i.e. integrals of operators such as kinetic energy, nuclear attraction, coulomb and exchange, with the basis functions). In this first part of the appendix, the stability of the results with respect to the variation of parameters concerning the grid and the parameters concerning the selection of the integrals is tested. For further tests, see also the extensive tests performed for lithium<sup>59</sup>, or tests for copper<sup>7</sup> and silver<sup>49</sup> ( $\vec{k}$ -points, smearing temperature). In tables IX and X, the binding energies are computed with the default grid and truncation parameters, and with an improved grid and two sets of stricter and thus more accurate truncation parameters.

The improved grid has roughly six times more sampling points than the default grid for the various structures. As is displayed in the tables, the grid has virtually no impact on the energy splitting. For Cl/Ni(111), the binding energy changes by at most  $0.2 mE_h$  for fcc, hcp and bridge site, and only for the top site an energy change of  $0.9 mE_h$  is observed, with respect to the default grid. This has, however, no impact as the top site is much higher in energy anyway. For K/Ni(111) the absolute value of the binding energy is shifted by  $0.7 mE_h$ , and the relative energies of the various sites are identical.

There are two truncation parameters in calculations when no Fock exchange is involved<sup>17</sup>: a general one ("ITOL 1") which leads to a neglect of all integrals with an overlap below a certain threshold (default:  $10^{-6}$ ), and a second parameter ("ITOL 2") which leads to the evaluation of the coulomb integrals at a lower level of accuracy by means of a multipolar expansion, if the overlap is below another threshold (default:  $10^{-6}$ ). As the results turned out to be more sensitive to these parameters, two sets of higher thresholds were used ( $10^{-7}$  for ITOL 1 and

2, and  $10^{-8}$  for ITOL 1 and 2). In the case of chlorine, the largest error is found for the splitting between fcc and hcp site: it ranges from 0.7 to  $2.1 mE_h$ , for the various parameters, with the fcc site always being more favorable. The bridge site is always clearly higher than the fcc site by 3.3 to  $4.2 mE_h$ , and the top site is much higher in energy. For K/Ni(111), the impact of these parameters is smaller, and for example, the splitting from the top site to the site closest in energy ranges from  $0.5 mE_h$  to  $0.8 mE_h$ .

As a whole, the impact of these computational parameters is certainly not negligible, but the conclusions are not affected. The fcc site is favored for Cl/Ni(111), with the hcp site being nearly degenerate. In the case of K/Ni(111), the top site is favored, with the other sites being very close in energy.

## APPENDIX B: BASIS SET DEPENDENCE OF THE RESULTS

The choice of the basis set is of high importance for the quality of the results. In this part of the appendix, the results of various tests are displayed, to investigate the dependence of the results on the basis set. These tests focus on nickel bulk, the clean surfaces, and Cl/Ni(111).

Firstly, one might consider reoptimizing the exponents for the clean surface, for example keeping the exponents of the inner layer like in the bulk and reoptimizing the exponents of the outermost layers. This would result (with a slab with three layers) in exponents of 0.12 (*sp*, instead of 0.13 for the bulk) and 0.38 (*d*, as in bulk nickel) for the outer layers. This is thus a tiny change only and the results are virtually identical, for example the surface energy per atom changes by  $0.6 mE_h$  which is negligible. If an outermost *sp*-exponent of 0.12 instead of 0.13 is used for the bulk, exactly the same results as in table I are obtained.

There is however a property which depends extremely strong on the basis set: the computed work function changes drastically when the outermost exponent is changed by a tiny value. For example, with the *sp*-exponent used for all the calculations (0.13), the work function of the Ni(100) surface is  $0.142 E_h$  (exp.<sup>60,61</sup>:  $0.192 E_h$ ), of the Ni(110) surface  $0.129 E_h$  (exp.<sup>60,61</sup>:  $0.185 E_h$ ), and of the Ni(111) surface  $0.155 E_h$  (exp.<sup>60,61</sup>:  $0.197 E_h$ ). This data is practically stable with respect to the number of layers (i.e. 3 layers are sufficient to obtain a stable number). When, however, for example, the outermost *sp*-exponent of the outer layers is changed from 0.13 to 0.12, the work function of the Ni(111) surface changes by  $0.01 E_h$  to  $0.165 E_h$ , and it further increases with smaller exponents (e.g.  $0.183 E_h$ , if the outermost *sp*-exponent of the outer layers is 0.10 instead of 0.13). Also, increasing this exponent leads to a lower work function. The same problem shows also up with other metals, such as for example copper or silver (and also when the

exponents of all the layers and not just the outermost layers are changed). It appears thus that the work function is a quantity which is not well described with a local basis set. The work functions may be qualitatively reasonable, but a quantitative comparison seems unadvised. Thus, also the work function data computed for Ag and the adsorption thereon<sup>49</sup> has to be considered with caution. A problem with computing work functions with a local basis set was already discussed earlier<sup>62</sup>.

The results thus indicate that the only property which appears to be strongly basis set dependent is the work function (total energy, surface energy, bulk modulus and lattice constant are essentially stable with respect to small variations in the basis set). Mulliken charge and magnetic moment are stable if an identical basis is used for all the nickel atoms in a slab. Of course, if basis sets of different type are used for the inner layer of a slab and the outermost layers, the Mulliken population also gets less reliable.

Further tests were performed for the adsorbate system Cl/Ni(111). One test was done by choosing a more tight outermost *sp*-exponent of 0.15 instead of 0.09 for chlorine. When a structural optimization is performed, virtually the same structural data as in table IV is obtained (the maximum deviation is 0.01 Å). The binding energy is lower by  $3mE_h$  because of the poorer chlorine basis set. However, what is important is that the energy splitting for the various sites remains practically identical (the binding energy is  $-0.1326 E_h$  for the fcc site,  $-0.1320 E_h$  for the hcp site,  $-0.1292 E_h$  for the bridge site, and  $-0.1151 E_h$  for the top site). Also, properties such as the population, magnetic moment and the relative position of the core levels with respect to the Fermi energy are essentially stable with respect to this change of the basis set (but again the work function changes strongly).

As a whole, the basis set needs of course to be carefully chosen. When this is done, the results for the geometry, energies, core eigenvalues, populations, and magnetic moments are reliable and not too strongly basis set dependent. The accurate determination of the work function, however, appears to be difficult with a local basis set.

---

<sup>1</sup> R. D. Diehl and R. McGrath, Surf. Sci. Rep. **23**, 43 (1996);  
R. D. Diehl and R. McGrath, J. Phys.: Condensed Matter **9**, 951 (1997).

<sup>2</sup> H. Over, Progr. in Surf. Sci. **58**, 249 (1998).

<sup>3</sup> C. Stampfl and M. Scheffler, Surf. Rev. Lett. **2**, 317 (1995);  
M. Scheffler and C. Stampfl, in: Handbook of Surface Science, Vol. 2: Electronic Structure, Editors: K. Horn and M. Scheffler, Amsterdam (1999).

<sup>4</sup> A. Zangwill, Physics at Surfaces, University Press, Cambridge (1988).

- <sup>5</sup> Y. Takata, H. Sato, S. Yagi, T. Yokoyama, T. Ohta, and Y. Kitajima, Surf. Sci. **265**, 111 (1992).
- <sup>6</sup> M. F. Kadodwala, A. A. Davis, G. Scragg, B. C. C. Cowie, M. Kerkar, D. P. Woodruff, R. G. Jones, Surf. Science **324**, 122 (1995).
- <sup>7</sup> K. Doll and N. M. Harrison, Chem. Phys. Lett. **317**, 282 (2000).
- <sup>8</sup> K. Doll and N. M. Harrison, Phys. Rev. B **63**, 165410 (2001).
- <sup>9</sup> L. Jia, Y. Wang and K. Fan, J. Phys. Chem. B **107**, 3813 (2003).
- <sup>10</sup> S. Wang and P. A. Rikvold, Phys. Rev. B **65**, 155406 (2002).
- <sup>11</sup> V. Blum, L. Hammer, K. Heinz, C. Franchini, J. Redinger, K. Swamy, C. Deisl and E. Bertel, Phys. Rev. B **65**, 165408 (2002).
- <sup>12</sup> Y. Wang, W. Wang, K. Fan and J. Deng, Surf. Sci. **487**, 77 (2001).
- <sup>13</sup> G. Kresse and J. Hafner, Surf. Sci. **459**, 287 (2000).
- <sup>14</sup> F. Mittendorfer and J. Hafner, Surf. Sci. **472**, 133 (2001).
- <sup>15</sup> A. Michaelides and P. Hu, J. Chem. Phys. **112**, 8120 (2000).
- <sup>16</sup> Q. Ge, S. J. Jenkins and D. A. King, Chem. Phys. Lett. **327**, 125 (2000).
- <sup>17</sup> V. R. Saunders, R. Dovesi, C. Roetti, M. Causà, N. M. Harrison, R. Orlando, C. M. Zicovich-Wilson CRYSTAL 98 User's Manual, Theoretical Chemistry Group, University of Torino (1998).
- <sup>18</sup> J. P. Perdew, K. Burke and M. Ernzerhof, Phys. Rev. Lett. **77**, 3865 (1996).
- <sup>19</sup> J. P. Perdew, J. A. Chevary, S. H. Vosko, K. A. Jackson, M. R. Pederson, D. J. Singh, and C. Fiolhais, Phys. Rev. B **46**, 6671 (1992).
- <sup>20</sup> B. Hammer, L. B. Hansen, and J. K. Nørskov, Phys. Rev. B **59**, 7413 (1999).
- <sup>21</sup> M. D. Towler, N. L. Allan, N. M. Harrison, V. R. Saunders, W. C. Mackrodt, E. Aprà, Phys. Rev. B **50**, 5041 (1994).
- <sup>22</sup> K. Doll, Euro. Phys. J. B **22**, 389 (2001).
- <sup>23</sup> The energies of the neutral atoms were computed as follows: the outermost Cl *sp*-shells were 0.315 and 0.119 instead of 0.294 and 0.090, yielding an energy of -459.9385  $E_h$ . For K, three diffuse *sp* shells (0.39, 0.21, 0.03) replaced the two used for the adsorption studies (0.29, 0.08), yielding an energy of -599.6672  $E_h$ . For the nickel atom, 7 additional even tempered diffuse functions in the range from 0.01 to 0.25 (*sp*), and 5 from 0.016 to 0.6 (*d*), were employed, the [5s4p1d] tight inner exponents were kept as in the bulk. Thus, as a whole a [12s11p6d] basis set was used. The PBE-energies were -1507.933  $E_h$  ( $d^8s^2$ ); (PW: -1508.311  $E_h$ ), and -1507.967  $E_h$  ( $d^9s^1$ ); (PW: -1508.346  $E_h$ ). The energies of the nickel atom were calculated with integer occupation numbers, the  $d_{z^2}$  and  $d_{x^2-y^2}$  orbital were singly occupied in the case of the  $d^8s^2$  state, and the  $d_{x^2-y^2}$  orbital in the case of the  $d^9s^1$  state.
- <sup>24</sup> R. McWeeny, J. Chem. Phys. **19**, 1614 (1951).
- <sup>25</sup> R. S. Mulliken, J. Chem. Phys. **23**, 1833 (1955).
- <sup>26</sup> D. Cook and B. Sutcliffe, Int. J. Quantum Chem. **60**, 1 (1996); R. McWeeny, Int. J. Quantum Chem. **60**, 3 (1996).
- <sup>27</sup> J. Neugebauer and M. Scheffler, Phys. Rev. B **46**, 16067 (1992).

- <sup>28</sup> E. G. Moroni, G. Kresse, J. Hafner and J. Furthmüller, *Phys. Rev. B* **56**, 15629 (1997).
- <sup>29</sup> C. E. Moore, Atomic Energy Levels, NSRDS-NBS 35 / Vol. I-III, Nat. Bur. Standards (Washington, DC, 1949, 1952, 1958).
- <sup>30</sup> R. L. Martin, P. J. Hay, *J. Chem. Phys.* **75**, 4539 (1981)
- <sup>31</sup> K. Raghavachari and G. W. Trucks, *J. Chem. Phys.* **91**, 1062 (1989).
- <sup>32</sup> J. Harris and R. O. Jones, *J. Chem. Phys.* **70**, 830 (1979).
- <sup>33</sup> T. V. Russo, R. L. Martin, and J. P. Hay, *J. Chem. Phys.* **101**, 7729 (1994).
- <sup>34</sup> J. Langlinais and J. Callaway, *Phys. Rev. B* **5**, 124 (1972).
- <sup>35</sup> C. S. Wang and J. Callaway, *Phys. Rev. B* **9**, 4897 (1974).
- <sup>36</sup> J. W. D. Connolly, *Phys. Rev.* **159**, 415 (1967).
- <sup>37</sup> H. C. Lu, E. P. Gusev, E. Garfunkel, and T. Gustafsson, *Surf. Sci.* **352-354**, 21 (1996).
- <sup>38</sup> F. Mittendorfer, A. Eichler and J. Hafner, *Surf. Sci.* **423**, 1 (1999).
- <sup>39</sup> W. Erley and H. Wagner, *Surf. Sci.* **66**, 371 (1977).
- <sup>40</sup> M. Funabashi, Y. Kitajima, T. Yokoyama, T. Ohta and H. Kuroda, *Physica B* **158**, 664 (1989).
- <sup>41</sup> M. Funabashi, T. Yokoyama, Y. Takata, T. Ohta, Y. Kitajima and H. Kuroda, *Surf. Sci.* **242**, 59 (1991).
- <sup>42</sup> L.-Q. Wang, Z. Hussain, Z. Q. Huang, A. E. Schach v. Wittenau, D. W. Lindle and D. A. Shirley, *Phys. Rev. B* **44**, 13711 (1991).
- <sup>43</sup> W.-X. Li, C. Stampfl and M. Scheffler, *Phys. Rev. B* **65**, 075407 (2002).
- <sup>44</sup> L. Pauling, The nature of the chemical bond and the structure of molecules and crystals, Cornell University Press (1960).
- <sup>45</sup> C. Kittel, Introduction to solid state physics, 7th edition, Wiley, New York, Chichester, Brisbane, Toronto, Singapore (1996).
- <sup>46</sup> M. D. Crapper, C. E. Riley, P. J. J. Sweeney, C. F. McConville, and D. P. Woodruff, *Europhys. Lett.* **2**, 857 (1986).
- <sup>47</sup> A. G. Shard, V. R. Dhanak and A. Santoni, *Surf. Sci.* **429**, 279 (1999).
- <sup>48</sup> A. G. Shard, V. R. Dhanak and A. Santoni, *Surf. Sci.* **445**, 309 (2000).
- <sup>49</sup> K. Doll, *Phys. Rev. B* **66**, 155421 (2002).
- <sup>50</sup> S. Chandavarkar and R. D. Diehl, *Phys. Rev. B* **38**, 12112 (1988).
- <sup>51</sup> D. Fisher, S. Chandavarkar, I. R. Collins, R. D. Diehl, P. Kaukasoina and M. Lindroos, *Phys. Rev. Lett.* **68**, 2786 (1992).
- <sup>52</sup> P. Kaukasoina, M. Lindroos, R. D. Diehl, D. Fisher, S. Chandavarkar, and I. R. Collins, *J. Phys.: Cond. Matter* **5**, 2875 (1993).
- <sup>53</sup> D. L. Adler, I. R. Collins, X. Liang, S. J. Murray, G. S. Leatherman, K.-D. Tsuei, E. E. Chaban, S. Chandavarkar, R. McGrath, R. D. Diehl and P. H. Citrin, *Phys. Rev. B* **48**, 17445 (1993).
- <sup>54</sup> Z. Huang, L. Q. Wang, A. E. Schach von Wittenau, Z. Hussain, and D. A. Shirley, *Phys. Rev. B* **47**, 13626 (1993).
- <sup>55</sup> R. Davis, X.-M. Hu, D. P. Woodruff, K.-U. Weiss, R. Dippel, K.-M. Schindler, Ph. Hofmann, V. Fritzsche and A. M. Bradshaw, *Surf. Sci.* **307**, 632 (1994).
- <sup>56</sup> X. Shi, D. Tang, D. Heskett, K.-D. Tsuei, H. Ishida, Y.



- Morikawa, and K. Terakura, Phys. Rev. B **47**, 4014 (1993).
- <sup>57</sup> M.-L. Shek, J. Hrbek, T. K. Sham, and G.-Q. Xu, Phys. Rev. B **41**, 3447 (1990).
- <sup>58</sup> D. M. Riffe, G. K. Wertheim, and P. H. Citrin, Phys. Rev. Lett. **64**, 571 (1990).
- <sup>59</sup> K. Doll, N. M. Harrison, and V. R. Saunders, J. Phys.: Condensed Matter **11**, 5007 (1999).
- <sup>60</sup> B. G. Baker, B. B. Johnson and G. L. C. Maire, Surf. Sci. **24**, 572 (1971).
- <sup>61</sup> H. B. Michaelson, J. Appl. Phys. **48**, 4729 (1977).
- <sup>62</sup> J. C. Boettger, U. Birkenheuer, S. Krüger, N. Rösch, and S. B. Trickey, Phys. Rev. B **52**, 2025 (1995).
- <sup>63</sup> K. A. Gschneidner, Jr., Solid State Phys. **16**, 276 (1964).
- <sup>64</sup> M. Aldén, H. L. Skriver, S. Mirbt and B. Johansson, Surf. Sci. **315**, 157 (1994).
- <sup>65</sup> L. Vitos, A. V. Ruban, H. L. Skriver and J. Kollár, Surf. Science **411**, 186 (1998).
- <sup>66</sup> C. L. Fu and A. J. Freeman, Journal de Physique C49, Colloque C8, 1625 (1988).
- <sup>67</sup> E. Wimmer, A. J. Freeman, and H. Krakauer, Phys. Rev. B **30**, 3113 (1984).

TABLE I. The ground state properties of bulk Ni.

	lattice constant $a_0$ [Å]	$E_{coh}$ [ $E_h$ ]	$B$ [GPa]	magnetic moment [ $\mu_B$ ]
PBE, this work	3.53	0.218 <sup>a</sup> 0.184 <sup>b</sup>	203	0.62
PW, this work	3.53	0.220 <sup>a</sup> 0.185 <sup>b</sup>	203	0.61
Ref. 28, LDA	3.43		255	0.59
Ref. 28, GGA	3.53		195	0.61
exp.	3.52 <sup>63</sup>	0.163 <sup>a</sup> , 0.164 <sup>b63</sup>	190 <sup>63</sup>	0.61 <sup>45</sup>

<sup>a</sup> energy with respect to a free nickel atom in its  $d^8s^2$  state  
<sup>b</sup> energy with respect to a free nickel atom in its  $d^9s^1$  state

TABLE II. The surface energy [ $\frac{E_h}{\text{surface atom}}$ ] of the low index nickel surfaces.

surface	PBE, this work	Ref. 38	Ref. 64	Ref. 65
(100)	0.038	0.031	0.039	0.036
(110)	0.056	0.046	-	0.049
(111)	0.028 (PW: 0.028)	0.024	0.033	0.026

TABLE III. Magnetic moments [ $\mu_B$ ] of the low index nickel surfaces, computed using a slab with 9 Ni layers.

layer	PBE, this work	PW, this work	Ref. 38 (9 layers, 3 surface layers on both sides are allowed to relax)	Ref. 64	Ref. 66 (7 layers)	Ref. 67 (7 layers)
(100) surface						
S	0.729		0.76	0.69		0.68
S-1	0.634		0.68	0.64		0.60
S-2	0.632		0.66	0.66		0.59
S-3	0.611			0.64		0.56
S-4	0.619					
(110) surface						
S	0.757		0.76			
S-1	0.637		0.66			
S-2	0.618		0.64			
S-3	0.620					
S-4	0.607					
(111) surface						
S	0.648 (relaxed: 0.649)	0.638	0.68	0.62	0.63	
S-1	0.658 (relaxed: 0.657)	0.649	0.65	0.67	0.64	
S-2	0.622 (relaxed: 0.622)	0.613	0.62	0.65	0.58	
S-3	0.617 (relaxed: 0.617)	0.604		0.63	0.58	
S-4	0.613 (relaxed: 0.613)	0.605				

TABLE IV. Adsorption of Cl on the Ni(111) surface.  $d_{\text{Cl-Ni top layer}}$  is the interlayer distance between the Cl layer and the top Ni layer,  $d_{\text{Cl-Ni nn}}$  is the bond length between Cl and nearest neighbor Ni.  $d_{N_{i1}-N_{i2}}$  is the distance between first and second nickel layer. The distance between second and third nickel layer  $d_{N_{i2}-N_{i3}}$  is held fixed at the bulk value (and for the thicker slabs also  $d_{N_{i3}-N_{i4}}$  and  $d_{N_{i4}-N_{i5}}$  are fixed at the bulk value). The adsorption energy is the difference  $E_{\text{Cl at Ni(111)}} - E_{\text{Ni(111)}} - E_{\text{Cl}}$ .

Site	$d_{\text{Cl-Ni top layer}}$ [Å]	$d_{N_{i1}-N_{i2}}$ [Å]	$d_{\text{Cl-Ni nn}}$ [Å]	$E_{\text{adsorption}}$ [ $\frac{E_h}{\text{Cl atom}}$ ]
		3 nickel layers		
fcc	1.84	2.02	2.34	-0.1358
hcp	1.85	2.02	2.35	-0.1351
bridge	1.90	2.02	2.27	-0.1325
top	2.14	2.02	2.14	-0.1177
		4 nickel layers		
fcc	1.83	2.02	2.33	-0.1338
hcp	1.84	2.02	2.34	-0.1336
bridge	1.89	2.02	2.27	-0.1307
top	2.14	2.02	2.14	-0.1159
		5 nickel layers		
fcc (single point calculation)				-0.1337
hcp (single point calculation)				-0.1331
exp. (ARPEFS) <sup>42</sup>	1.837	1.926	2.332	
exp. (SEXAFS, XSW) <sup>40,41</sup>	1.92, 1.83	2.03, 2.02	2.40, 2.33	

TABLE V. Charge and position of the 3s eigenvalue for Cl and the 3s and 3p eigenvalues for K on different adsorption sites, relative to the Fermi energy. For chlorine, the peaks are at slightly different positions for majority and minority bands, for potassium they are at the same position.

site	charge, in $ e $	3s level, relative to $E_F$ [ $E_h$ ]	3p level, relative to $E_F$ [ $E_h$ ]
		Cl on Ni:	
fcc	-0.050	-0.589 (majority spin); -0.586 (minority spin)	
hcp	-0.046	-0.586 ; -0.584	
bridge	-0.068	-0.580 ; -0.578	
top	-0.152	-0.537 ; -0.535	
		K on Ni:	
fcc	+0.294	-1.178 (both spins)	-0.583 (both spins)
hcp	+0.295	-1.178	-0.582
bridge	+0.291	-1.178	-0.583
top	+0.269	-1.179	-0.583

TABLE VI. Mulliken spin and charge population for Cl/Ni(111), on different adsorption sites, extracted from calculations with 5 nickel layers. The population for the nickel atoms in the individual layers is given. The number in parenthesis gives the number of atoms which are identical because of symmetry and thus have an identical population. The left column corresponds to that atom(s) in the layer which is closer to the chlorine adsorbate. For example, in the fcc case, all three nickel atoms of a supercell in the first and second layer have the same distance and thus the population is identical, but one atom in the third layer is closer than the other two atoms resulting in two different values for the spin population. In the case of the clean slab, all atoms within one layer are degenerate and thus only one number is displayed.

site	1 <sup>st</sup> layer	2 <sup>nd</sup> layer	3 <sup>rd</sup> layer	4 <sup>th</sup> layer	5 <sup>th</sup> layer	Cl
spin						
fcc	0.67 (3 atoms)	0.64 (3 atoms)	0.59 (1 atom) 0.64 (2 atoms)	0.66 (3 atoms)	0.65 (3 atoms)	0.08
hcp	0.68 (3 atoms)	0.68 (1) 0.63 (2)	0.62 (3)	0.66 (3)	0.63 (1) 0.66 (2)	0.08
bridge	0.66 (2) 0.73 (1)	0.67 (1) 0.63 (2)	0.60 (1) 0.63 (2)	0.66 (2) 0.65 (1)	0.64 (1) 0.66 (2)	0.08
top	0.55 (1) 0.76 (2)	0.64 (3)	0.62 (3)	0.67 (1) 0.64 (2)	0.65 (3)	0.04
clean slab	0.66	0.66	0.63	0.66	0.66	
charge						
fcc	27.97 (3)	28.02 (3)	28.00 (1) 28.00 (2)	28.05 (3)	27.95 (3)	17.05
hcp	27.97 (3)	28.02 (1) 28.00 (2)	28.00 (3)	28.05 (3)	27.95 (1) 27.95 (2)	17.05
bridge	28.00 (2) 27.90 (1)	28.02 (1) 28.01 (2)	28.00 (1) 28.00 (2)	28.05 (2) 28.05 (1)	27.95 (1) 27.95 (2)	17.07
top	28.12 (1) 27.84 (2)	28.02 (3)	28.00 (3)	28.05 (1) 28.05 (2)	27.95 (3)	17.15
clean slab	27.95	28.05	28.00	28.05	27.95	

TABLE VII. Adsorption of K on the Ni(111) surface.  $d_{K-Ni1a}$  is the interlayer distance between the K layer and the layer made of those nickel atoms in the first layer closest to the K layer.  $d_{Ni1b-Ni2}$  is the distance between the layer made of those nickel atoms of the first layer which have moved away from the adsorbate and the second Ni layer.  $\delta = d_{Ni1a-Ni1b}$  is the rumpling within the first layer.  $d_{K-Ni\ nn}$  is the bond length between K and nearest neighbor Ni. Again, the distance between second and third nickel layer  $d_{Ni2-Ni3}$  is held fixed at the bulk value. The adsorption energy is the difference  $E_{K\ at\ Ni(111)} - E_{Ni(111)} - E_K$ .

Site	$d_{K-Ni1a}$ [Å]	$d_{Ni1b-Ni2}$ [Å]	$\delta$ [Å]	$d_{K-Ni\ nn}$ [Å]	$E_{adsorption}$ [ $\frac{E_h}{K\ atom}$ ]
without rumpling					
fcc	2.71	2.01	0	3.07	-0.0532
hcp	2.70	2.01	0	3.06	-0.0531
bridge	2.70	2.01	0	2.98	-0.0531
top	2.76	2.01	0	2.76	-0.0528
with rumpling					
fcc	2.63	1.99	+0.07	3.06	-0.0536
hcp	2.63	1.99	+0.07	3.06	-0.0535
bridge	2.65	1.97	+0.07	2.99	-0.0535
top	2.68	1.93	+0.11	2.79	-0.0544
experiment					
exp. (LEED) <sup>51,52</sup>	2.70±0.04	1.90±0.03	0.12±0.02	2.82±0.04	
exp. (SEXAFS) <sup>53</sup>				2.92±0.02	
exp. (ARPEFS) <sup>54</sup>		1.90±0.04	0.00±0.03	3.02 ± 0.01	
exp. (PhD) <sup>55</sup>		1.86 ± 0.06	0.01±0.09	2.87±0.06	

TABLE VIII. Mulliken spin and charge population for K/Ni(111), on different adsorption sites, extracted from calculations with 3 nickel layers. The population for the nickel atoms in the individual layers is given. The left column corresponds to that atom in the layer which is closest to the potassium adsorbate. For example, in the top case, one atom in the first layer is closer than the other three atoms resulting in two different values for the population. In the case of the clean slab, all atoms within one layer are degenerate and thus only one number is displayed. Also, when the populations were found to be identical, only one number was displayed (usually from the second Ni layer on, marked with 'all').

site	1 <sup>st</sup> layer		2 <sup>nd</sup> layer	3 <sup>rd</sup> layer	K
	spin				
fcc	0.58 (3 atoms)	0.62 (1 atom)	0.68 (all)	0.66 (all)	0.001
hcp	0.59 (3 atoms)	0.61 (1 atom)	0.68 (all)	0.66 (all)	0.001
bridge	0.58 (2 atoms)	0.61 (2 atoms)	0.68 (all)	0.66 (all)	0.000
top	0.55 (1 atom)	0.61 (3 atoms)	0.68 (3 atoms)	0.69 (1 atom)	-0.003
clean slab	0.66		0.69	0.66	
	charge				
fcc	28.04 (3 atoms)	28.00 (1 atom)	28.10 (all)	27.95 (all)	18.71
hcp	28.04 (3 atoms)	28.00 (1 atom)	28.10 (all)	27.95 (all)	18.71
bridge	28.05 (2 atoms)	28.00 (2 atoms)	28.10 (all)	27.95(all)	18.71
top	28.08 (1 atom)	28.00 (3 atoms)	28.10 (all)	27.95 (all)	18.73
clean slab	27.95		28.09	27.95	

TABLE IX. Binding energies for Cl/Ni(111), extracted from calculations with 3 nickel layers, as a function of the computational parameters. The geometry was held fixed at the one optimized with the default parameters (table IV).

site	default grid, default ITOL ( $10^{-6}$ , $10^{-6}$ )	better grid, default ITOL ( $10^{-6}$ , $10^{-6}$ )	default grid, higher ITOL ( $10^{-7}$ , $10^{-7}$ )	default grid, even higher ITOL ( $10^{-8}$ , $10^{-8}$ )
fcc	-0.1358	-0.1357	-0.1359	-0.1357
hcp	-0.1351	-0.1349	-0.1338	-0.1339
bridge	-0.1325	-0.1325	-0.1317	-0.1317
top	-0.1177	-0.1186	-0.1180	-0.1179

TABLE X. Binding energies for K/Ni(111), extracted from calculations with 3 nickel layers, as a function of the computational parameters. The geometry was held fixed at the one optimized with the default parameters (table VII).

site	default grid, default ITOL ( $10^{-6}$ , $10^{-6}$ )	better grid, default ITOL ( $10^{-6}$ , $10^{-6}$ )	default grid, higher ITOL ( $10^{-7}$ , $10^{-7}$ )	default grid, even higher ITOL ( $10^{-8}$ , $10^{-8}$ )
fcc	-0.0536	-0.0529	-0.0534	-0.0533
hcp	-0.0535	-0.0528	-0.0532	-0.0531
bridge	-0.0535	-0.0528	-0.0532	-0.0532
top	-0.0544	-0.0537	-0.0539	-0.0541

FIG. 1. The threefold hollow structures considered for Cl, adsorbed on the Ni(111) surface, at a coverage of one third of a monolayer,  $(\sqrt{3} \times \sqrt{3})R30^\circ$  unit cell. The nickel atoms in the top layer are displayed by open circles. The displayed chlorine adsorption sites are the threefold hollow sites (fcc or hcp hollow, filled circles). Note that these threefold hollow sites can not be distinguished in this figure. The ratio of the radii is chosen according to the computed values, i.e. using a nickel radius of 1.25 Å and a chlorine radius of 1.09 Å. The top site would be vertically above a nickel atom, the bridge site vertically above a point which is in the middle between two neighboring nickel atoms.

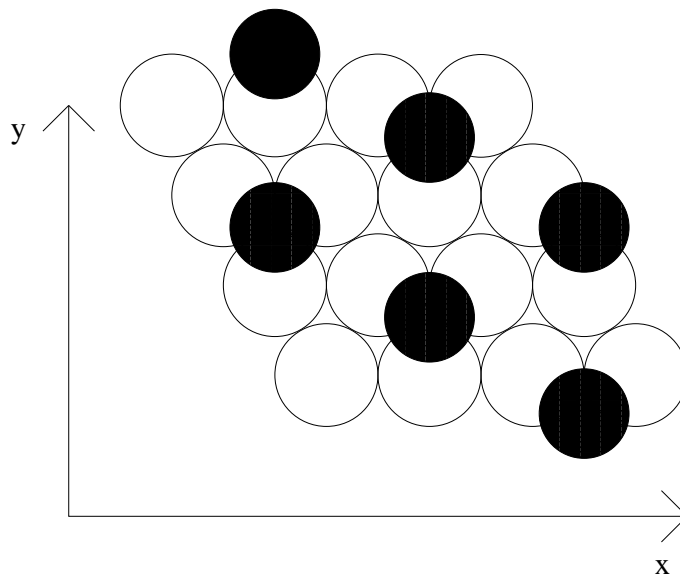


FIG. 2. Potassium, adsorbed on the Ni(111) surface, at a coverage of one fourth of a monolayer,  $(2 \times 2)$  unit cell. The nickel atoms in the top layer are displayed by open circles. The displayed potassium adsorption site is the top site vertically above the nickel atoms (filled circles). The ratio of the radii is chosen according to the computed values, i.e. using a nickel radius of  $1.25 \text{ \AA}$  and a potassium radius of  $1.54 \text{ \AA}$ .

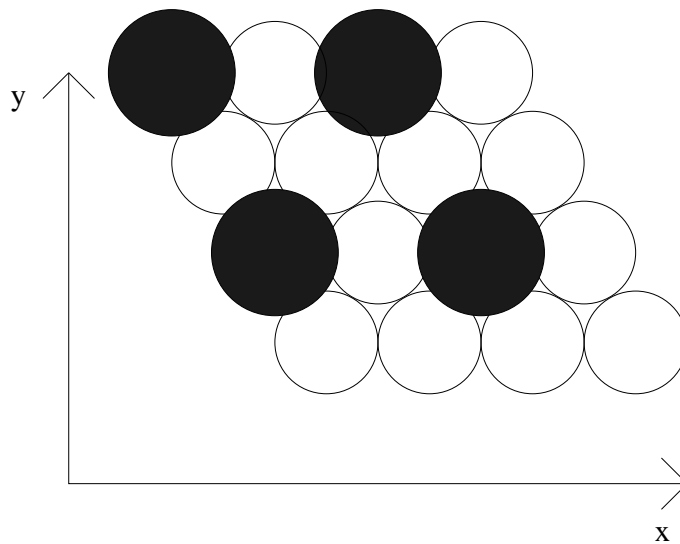
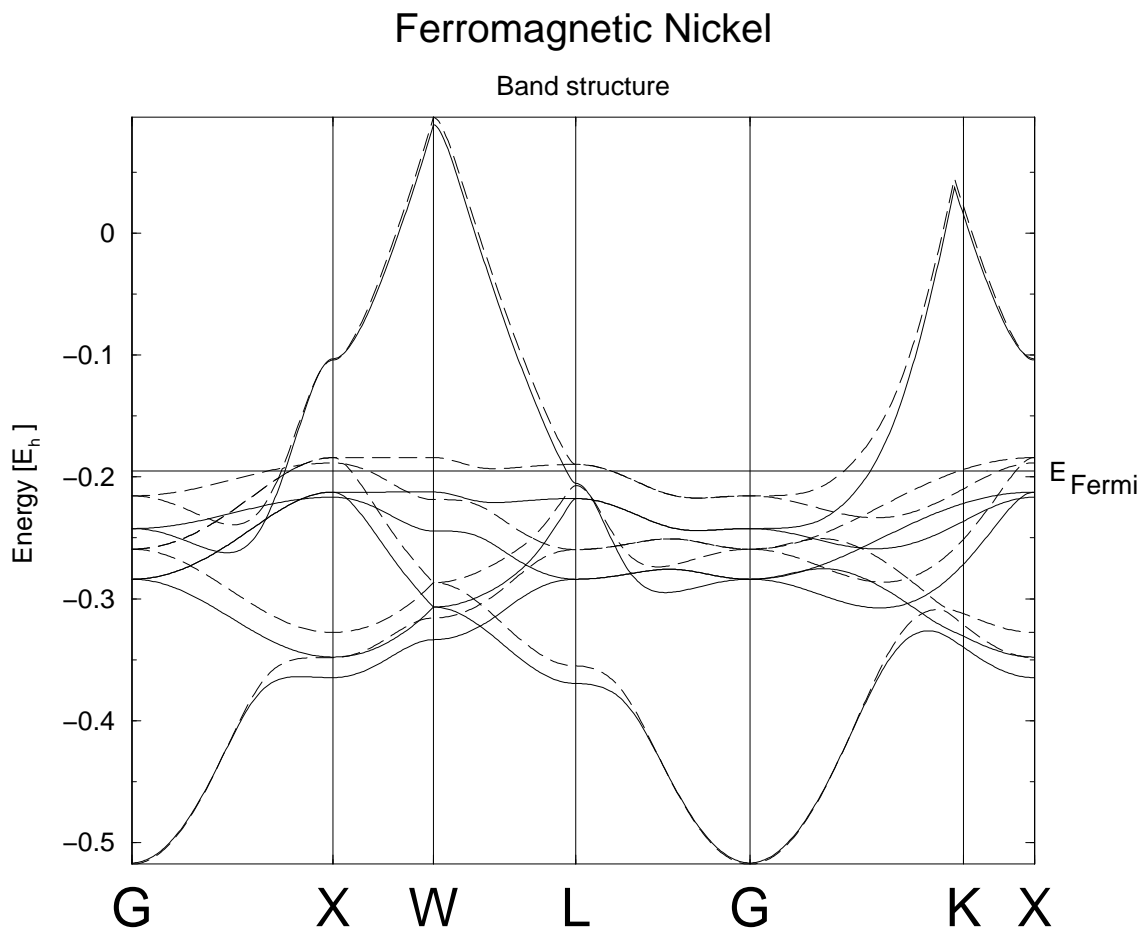


FIG. 3. Band structure of ferromagnetic nickel, with the PBE functional. The majority bands are drawn with full lines, the minority bands with dashed lines.





# Ni(111)( $\sqrt{3} \times \sqrt{3}$ )–Cl, fcc adsorption site

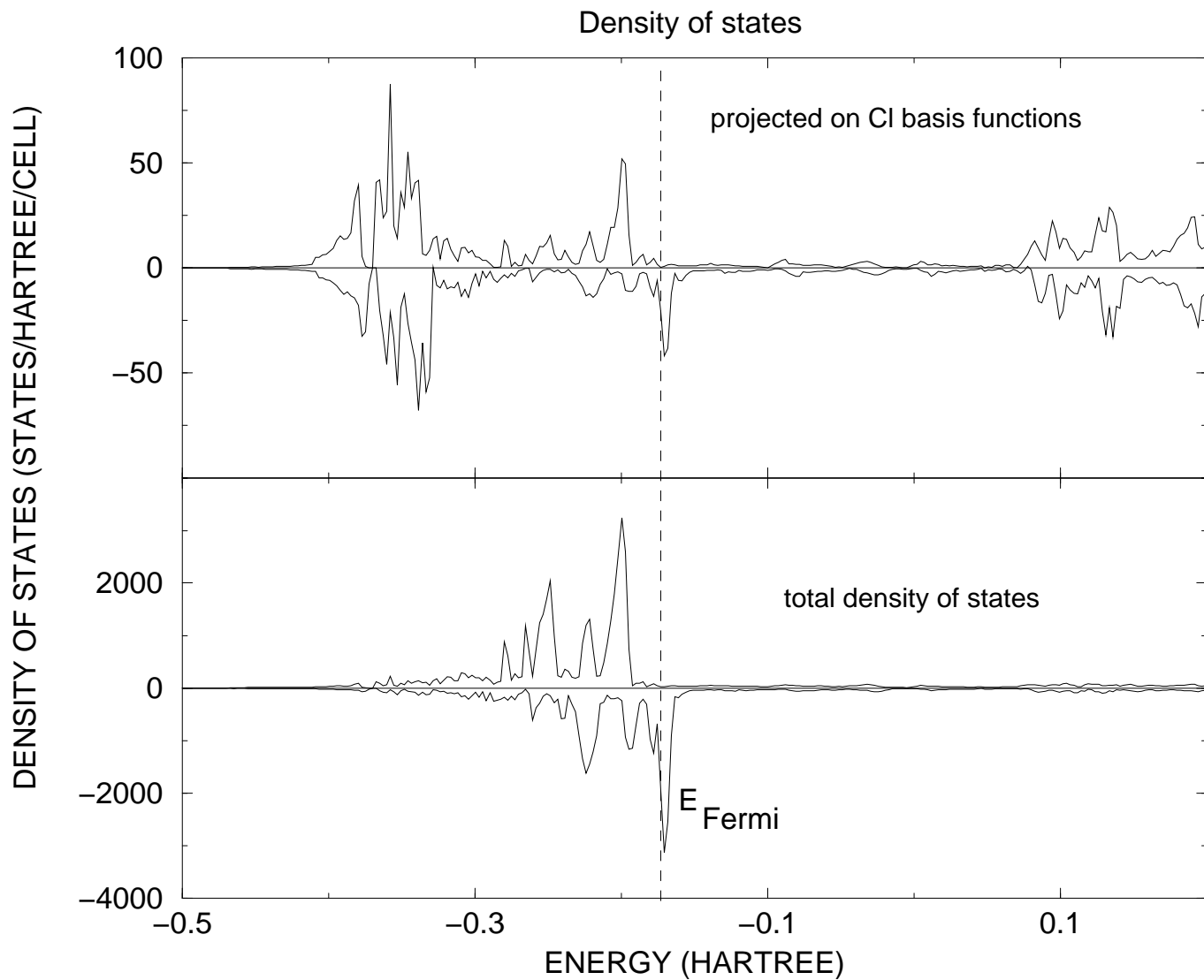


FIG. 4. The density of states, projected on the chlorine basis functions, (upper two graphs); and projected on all basis functions (lower two graphs), for majority (first and third graph) and minority band (second and fourth graph).

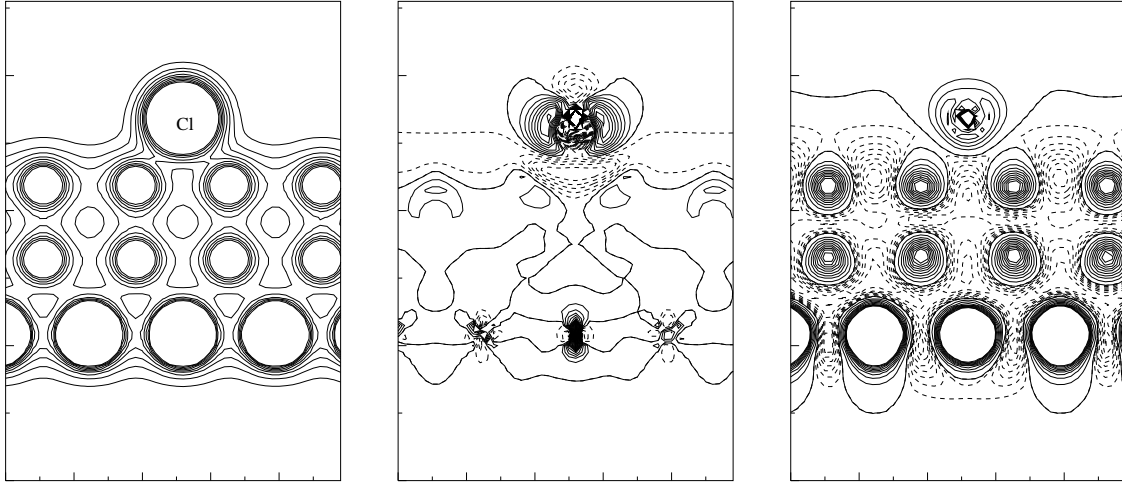


FIG. 5. Charge density (left), charge density difference (middle) and spin density (right) for Cl on Ni(111), from a three-layer slab, fcc site. The charge density is displayed with full lines, increasing in steps of 0.01, from 0 onwards. The charge density difference (charge of adsorbate system minus charge of a layer of chlorine atoms minus charge of a clean nickel surface) is in steps of 0.001, excess negative charge is displayed with full lines (from 0 onwards), electron depletion with dashed lines (from -0.001 onwards). Positive spin density is displayed with full lines, increasing from 0 in steps of 0.001. Negative spin density is displayed with dashed lines, decreasing from -0.0002 in steps of -0.0002. The plane goes through the center of the Cl adsorbate, and through the nickel atom in the third layer vertically under the chlorine, and through the nearest neighbors of this nickel atom in the third layer.

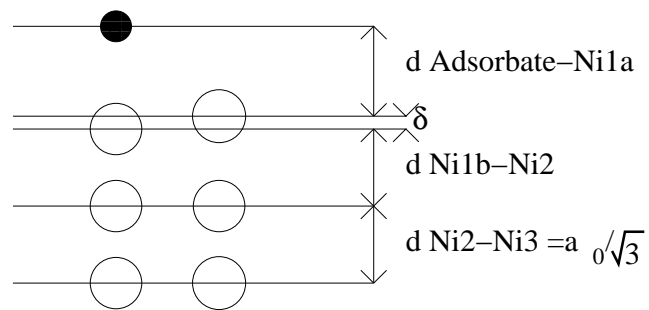


FIG. 6. Geometrical parameters for the adsorption studies.

# Ni(111)(2 x 2)-K, top adsorption site

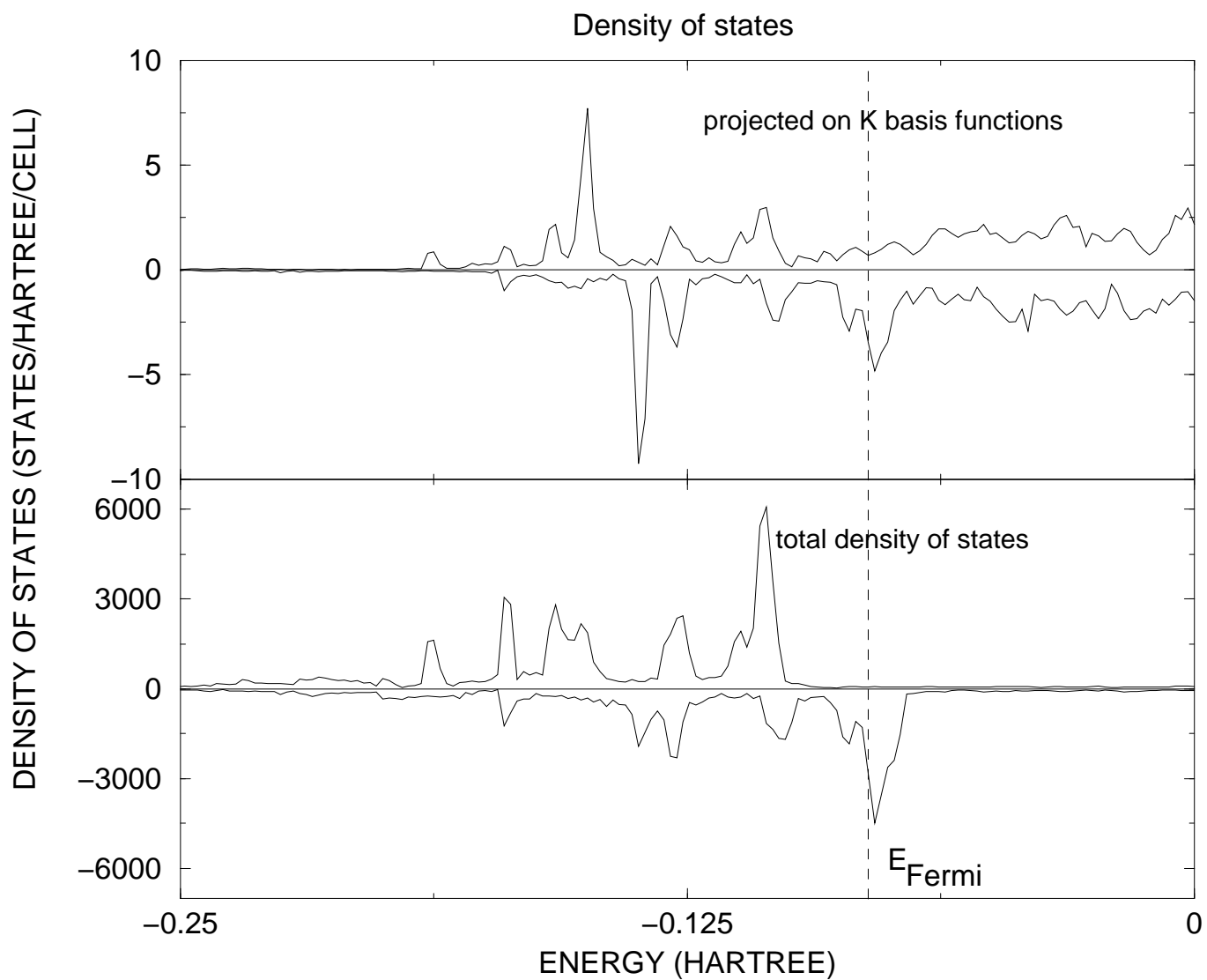


FIG. 7. The density of states, projected on the potassium basis functions, (upper two graphs); and projected on all basis functions (lower two graphs), for majority (first and third graph) and minority band (second and fourth graph).

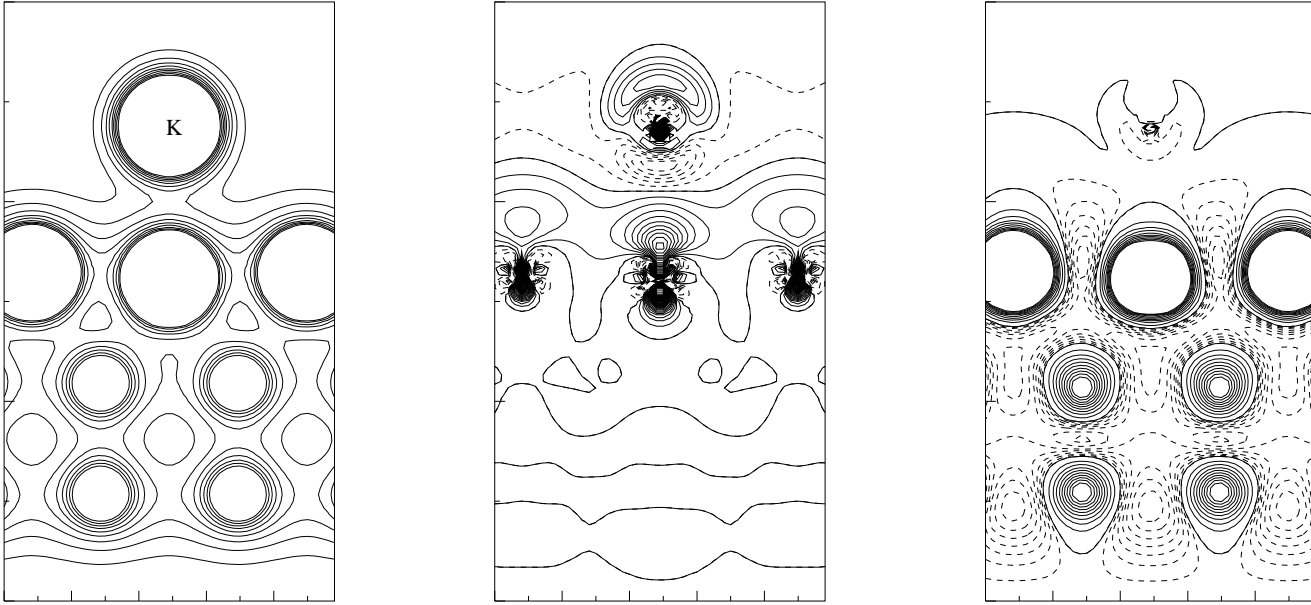


FIG. 8. Charge density (left), charge density difference (middle) and spin density (right) for K on Ni(111), from a three-layer slab, top site. The charge density is displayed with full lines, increasing in steps of 0.01, from 0 onwards. The charge density difference (charge of adsorbate system minus charge of a layer of potassium atoms minus charge of a clean nickel surface) is in steps of 0.001, excess negative charge is displayed with full lines (from 0 onwards), electron depletion with dashed lines (from -0.001 onwards). Positive spin density is displayed with full lines, increasing from 0 in steps of 0.001. Negative spin density is displayed with dashed lines, decreasing from -0.0002 in steps of -0.0002. The plane goes through the center of the K adsorbate, and through the nickel atom vertically below, and through the nearest neighbors of this nickel atom in the first layer.